Structural and Optical Properties of Colloidal $Cuinse_2$ Nanocrystals and its Thermally Evaporated Thin Films for Low-Cost Photovoltaics

Mohsen Ghali

Laboratory of Nanophotonics, Physics Department, Faculty of Science, Kafrelsheikh University, 33516 Kafrelsheikh, Egypt

We report on the synthesis of colloidal $CuInSe_2$ (CIS) nanocrystals NCs using simple solution-based method. The tetragonal phase $CuInSe_2$ NCs grow in the shape of nanoparticles with an average diameter of 30 nm. The band gap of the grown $CuInSe_2$ NCs is determined to be 1.09 eV. Furthermore, a successful deposition of the grown $CuInSe_2$ NCs in thin film form by vacuum thermal evaporation on Indium-tin-Oxide (ITO) substrates is achieved. The deposition process has been followed by thermal annealing in vacum, for only 5 minutes, at different temperatures (300-346 ^0C). We found a strong dependence of the structural, morphologies and optical absorption coefficient of the prepared CIS NCs films on annealing temperature. The formed CIS NCs films have been characterized using UV–Vis-NIR spectroscopy; scanning/transmission electron microscopy (SEM)/(TEM); energy dispersive X-ray analysis (EDX) and X-ray diffraction (XRD) techniques. Optical properties of CIS films were quantified using developed theoretical model based on transmission and reflectance measurements. A remarkable enhancement of the optical absorption coefficient (α~ $3x10^5$ cm^{-1}) of the formed CIS NCs films with annealing was demonstrated and suggested the potential use of colloidal CIS for photovoltaic as an active light harvesting material for low-cost solar cells devices.

1. Introduction

Thin film solar cells based on effective light absorbing I-III-VI_2 semiconductors, like CuInSe (CIS) and CuInGaSe (CIGS), are well known to be stable under long term light excitation with nearly 20% solar energy conversion efficiencies [1]. Up-to now $CuInSe_2$ still on the top list of materials for photovoltaics which act as an efficient solar radiation absorber. In recent years, interest has increased regarding the use of (CIS) compounds as materials for thin film photovoltaic solar cells because of their unique high theoretical efficiency of approximately 24.8% [1]. Moreover, the $CuInSe_2$ material has extraordinary radiation stability [2,3] and can form heterojunctions with materials such as ZnO, CdS and CdZnS with maximum efficiencies as yet are of 22.6% to 28.9% [4-6]. The CIS films possess certain exceptional material characteristics including a direct band-gap of 1.04 eV and a high optical absorption coefficient (~10^5 cm^{-1}) which is an essential requirement for or solar cell absorber applications. It should

be mentioned that CIS photoabsorber layer less than 1 µm thick can absorb more than 90% of the photon energy above its optical band gap. Because these films can be prepared with n- and p-type conductivity, there is potential for both a homo- and heterojunction [3]. Traditionally, CIS materials in state-of- the art devices are deposited using multi-stage co-evaporation and usually by the two-step process of sputtering and selenization. Such type of fabrication technology is very costly and requires sophisticated and expensive vacum equipments, besides the difficulty to achieve controlled stoichiometry of CIS materials over large devices area. In details, the typical method of depositing Thin films of CIS is based on to what so called three-source vacum evaporation method, followed by selenization (e.g., using H_2Se vapor) [7] where the elemental constituents of the CIS material i.e., Cu, In, and Se are co-evaporated in a controlled manner under high vacuum, then annealed in H_2Se gas [8] or in Se vapor atmosphere at elevated temperatures (around 500°C) [1]. The composition of the finished film depends on the thermal profile and diffusion from the substrate, as well as on the initial deposition. However, the selenization process either by using H_2Se gas or Se vapor is highly toxic to human body and environment. To achieve further commercial success for $CuInSe_2$-based photovoltaics and to reduce the cost of these solar cells, it is necessary to mass-produce quality $CuInSe_2$ films via a low-cost and environmentally-friendly process [6].

Compared with vacum-based methods, solution-based technique offer low-cost and scalability advantages. However, to the best of our knowledge, there are few reports on the synthesis of $CuInSe_2$ nanocrystals (NCs) films using solution-processed methods. Fabrication of thin film solar cells using solution-based processes are expected to be a potential substitute for all vacum-based technology of thin film solar cells.

Herein, we report on the colloidal synthesis of $CuInSe_2$ NCs powder and thin films with a primary particle size of ~30 nm using wet-chemistry method, and its nearly continuous thermally evaporated thin film. Moreover, we study the dependence of the structure, optical and morphologies on the annealing temperature of the $CuInSe_2$ films, without any selenization, where the CIS samples are formed upon annealing in *vacum* not in Selenium atmosphere as traditionally used. The $CuInSe_2$ films were annealed thermally in high vacuum, at different temperatures (up to 346^0C). We found the morphology, the structure and the absorption coefficient of the prepared CIS films to be dependent strongly on the annealing temperature. A high absorption coefficient of $\sim 3x10^{-5}$ cm^{-1} has been obtained for CIS films with thickness of only 160 nm when the annealing temperature reaches 346^0C.

2. Experimental details

2.1. Development of a simple home-made nitrogen-gas filled "glove box"

In order to prepare the $CuInSe_2$ nanocrystals using colloidal chemistry, it was crucial to synthesis the crystals in Air-free atmosphere (e.g., nitrogen gas environment) in order to avoid oxidation of the resultant materials. Moreover, the chemical reactants which are used for the synthesis process are highly sensitive to air and should be unpackaged (then kept) in inert gas environment. For these reasons it was crucial to have a nitrogen gas-filled glove box in our laboratory. We have succeeded to design, fabricate and test a simple home-made box for this reason as seen in Fig.(1).

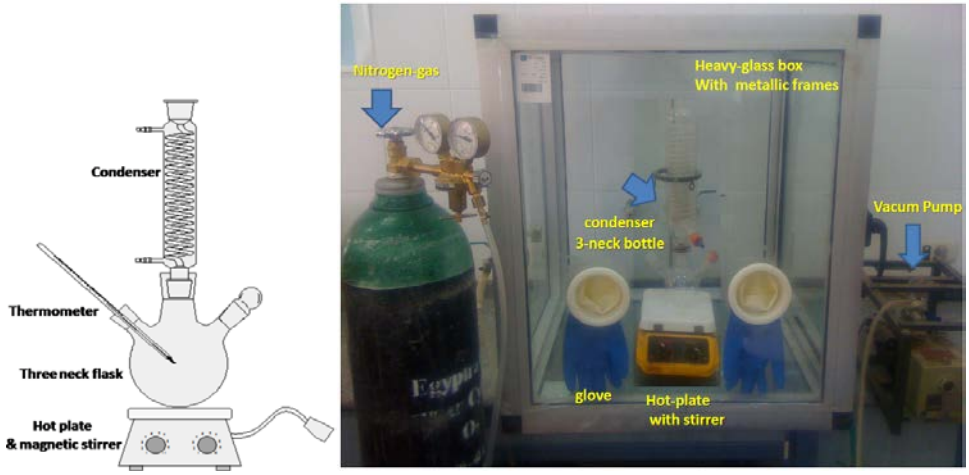

Figure (1): (left) Three-neck flask apparatus used for the growth of colloidal CuInSe nanocrystals. (right) A photo of our home-made simple nitrogen-gas filled box. A three-neck flask mounted on hot-plate magnetic stirrer is installed inside the box in order to make the synthesis process of CIS nanocrystals possible without oxidation.

As shown in Fig.(1) our box mainly includes:

1- Heavy duty glass box with metallic frames and complete isolation.
2- Commercially used two gloves which are mounted inside the front window of the system using Teflon with special epoxy.
3- High purity nitrogen gas source
4- Single stage rotary vacum pump

We put huge effort to isolate the box against leakage. We have used both the vacum pump and the nitrogen gas to pump and purge the system, respectively. After each pump/purge cycle, we were checking the leakage rate inside the box, until it reached the lowest level possible for moisture and Oxygen contents ~300 ppm).

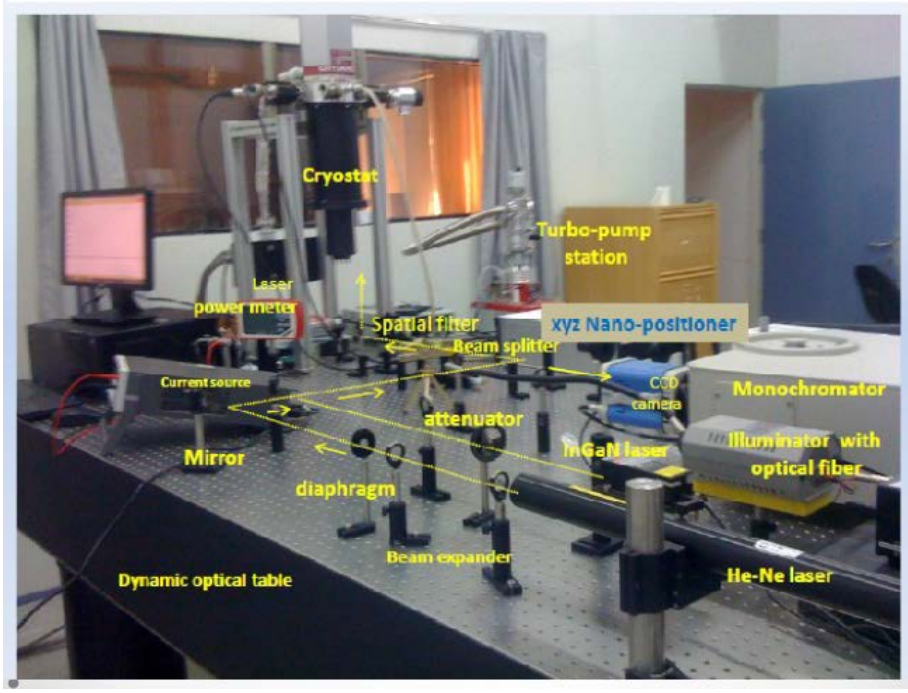

Figure (2): High resolution micro-photoluminescence (PL), absorption and transmittance technique.

2.2. Building an optical absorption and photoluminescence set up

In order to get access to optical properties of our grown CIS NCs we have build our optical absorption/transmission and photoluminescence (PL) set-up. The set-up is shown in Fig.2 along with its basic components including optical components (lenses, laser, Cryostat etc.). In other experiments, the transmittance/reflectance spectra were measured using a UV-Vis-NIR spectrometer (Shimadzu 2600/2700) where quantitative information on absorption coefficients (α) and the band gap energy (E_g) of the films were extracted. Moreover, the size and morphology of the as-synthesized $CuInSe_2$ NCs were characterized using Transmission Electron Microscope (TEM, Joel 100). For this purpose, the nanocrystals were dispersed in hexane and deposited on a TEM copper grid. The crystalline structure of the $CuInSe_2$ NCs was determined using X-ray diffraction XRD (Shimadzu 6000-XRD), and the optical properties were measured using a UV-Vis-NIR spectrometer (Shimadzu 2600/2700). The composition of thin film was determined using Energy-dispersive X-ray (EDX) analysis.

2.3. Synthesis of $CuInSe_2$ Nanocrystals

$CuInSe_2$ NCs were synthesized by reacting CuCl, $InCl_3$ and Se in Oleylamine (OLA) at an elevated temperature of 260 °C in N_2 gas atmosphere according to the general chemical equation [9]:

$$CuCl + InCl_3 + 2Se \xrightarrow{\text{oleylamine+heat}} CuInSe_2 \text{ nanocrystals} + \text{byproducts}$$

All manipulations were performed using our home-made nitrogen-gas filled glove box as shown in Fig.(1). In details: A 25 ml three-neck round bottom flask was purged three times by repeated cycles of vacuum and back-filling with N_2 gas. Then 0.049 g of CuCl, 0.11 g of $InCl_3$ and 5 ml of OLA were added to the flask under N_2 atmosphere. After that the temperature was raised to 72°C for 30 minutes, and 1 ml of 1 molar Se powder in OLA was rapidly injected into the reaction mixture with continuous stirring. The solution was subsequently heated up to 130° C. Then, the temperature was held at 260°C for 30 minutes until the reaction was completed. After reaction, the mixture was allowed to cool down to 60° C, and then 15 ml of the non-polar solvent (chloroform) was added to quench the reaction and disperse the particles. Finally, a 7.5 ml of the miscible anti-solvent ethanol was added to precipitate the particles before collection by centrifuge. The nanocrystal products were then purified by precipitation with excess ethanol followed by centrifugation at 5000 rpm for 10 min. After such a washing step, the supernatant contains unreacted precursor and byproducts is discarded. The nanocrystals are in the precipitate. The nanocrystals are then redispersed in 10 mL of chloroform and centrifuged at 4000 rpm for 5 min to remove poorly capped nanocrystals and large particulates, which settle during centrifugation. The well-capped nanocrystals remain dispersed in the supernatant. The precipitate is discarded and a small amount of OLA (0.2 mL) is subsequently added to the supernatant to ensure complete surface passivation of the nanocrystals. To remove excess capping ligands and remaining impurities, the product is again precipitated using 5 mL of ethanol and centrifuged at 8000 rpm for 10 min, then redispersed in chloroform. This process is done three times to obtain a high-purity product. The isolated nanocrystals disperse in hexane.

2.4. Deposition of $CuInSe_2$ thin Films

The $CuInSe_2$ thin films were deposited onto ITO-coated glass substrate by single source vacuum thermal evaporation method using vacum thermal evaporator unit (model Quaternium-70), where the grown CIS NCs powder is heated in open boat made of Molybdenum material until its vapor condenses in form of thin film on the cold substrate surface and on the vacuum chamber walls (ultimate pressure inside the chamber reaches $2x10^{-6}$ torr).

3. Results and Discussions

3.1. Structural analysis

The crystal structures of the as-synthesized $CuInSe_2$ NCs have been examined using X-ray diffraction (XRD). As shown in Fig.(3), the experimental XRD data matches well with the standard XRD patterns for $CuInSe_2$ material (ICDD 04-006-3637), indicating that $CuInSe_2$ NCs crystallize in the tetragonal structure (space group I-42d: a=b=5.76 Å, c=11.59 Å). The peaks at 26.81^0, 44.56^0,

52.71°, 64.48°, and 71.45° can be indexed to the (112), (220), (312), (400) and (332) planes of tetragonal $CuInSe_2$, respectively. There are no observable peaks for other binary or ternary impurities such as $CuSe_2$, $InSe_2$ or other secondary phases of $CuInSe_2$ system, etc. Furthermore, the peak intensity suggests that the powder contains large number of $CuInSe_2$ crystallites having preferred orientation along (112) direction.

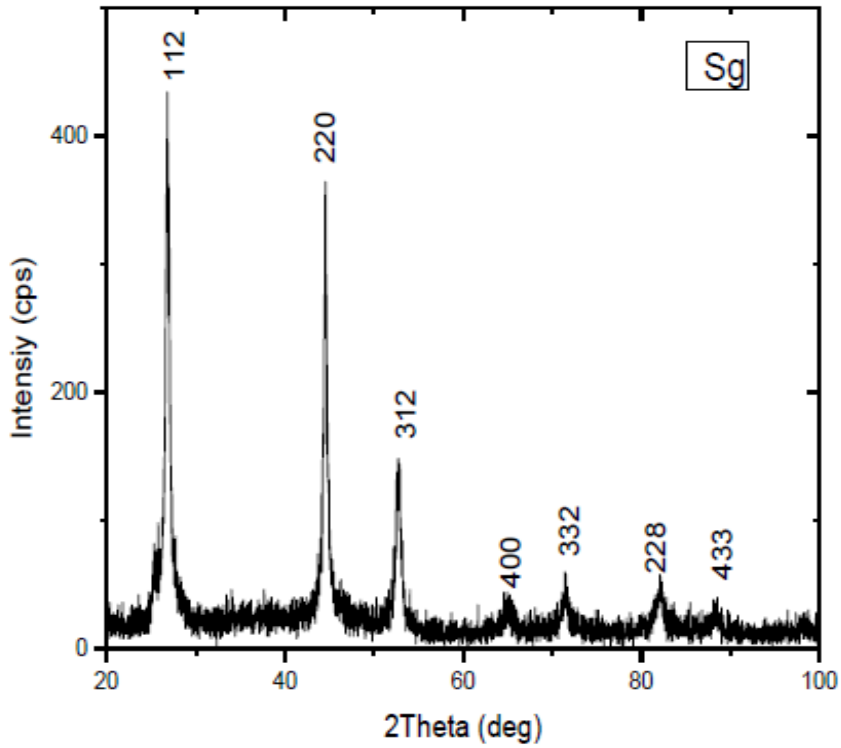

Figure (3): X-ray diffraction of our successfully grown CIS nanocrystals powder. The crystallographic planes are shown on the top of each peak.

Table 1: list of ‘‘d’’ spacings of $CuInSe_2$ NCs powder from XRD measurements.

2θ °	**d-spacing [Å]**	**Rel. Int. [%]**	**Plane**
26.81	3.321	100	112
44.56	2.031	83	220
52.71	1.734	34	312
64.48	1.434	10	400
71.45	1.318	13	332
82.11	1.172	8	228
88.55	1.103	9	433

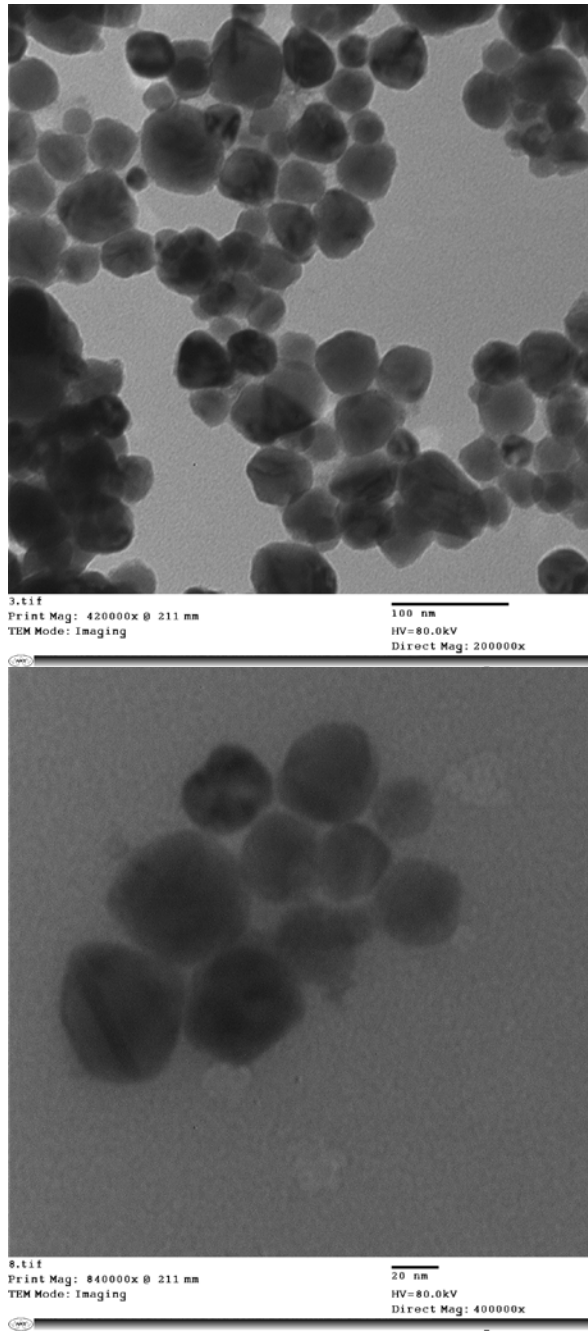

Figure (4): TEM image of our grown $CuInSe_2$ nanocrystals at different magnifications which shows average size of ~ 30 nm.

From Scherer's equation, $D = \frac{0.94\lambda}{\beta cos\theta}$ [10], we estimate the average particle size to be D= 35 nm where λ is X-ray wavelength, β is the full width at half maximum (FWHM) in radians, and θ is the Bragg angle.

3.2. Morphology of $CuInSe_2$ Nanocrystals and Films

We investigated the morphology of the $CuInSe_2$ NCs using Transmission Electron Microscopy (TEM) where a tetragonal-phase character of $CuInSe_2$ NCs can be seen in Fig.(4). As shown in Fig.(4) the as-synthesized product forms individually separated nanoparticles with minor sign of agglomeration, and with diameter of ~30 nm, in agreement with that calculated from the XRD data. The as-synthesized NCs have in average a uniform-like shape and size.

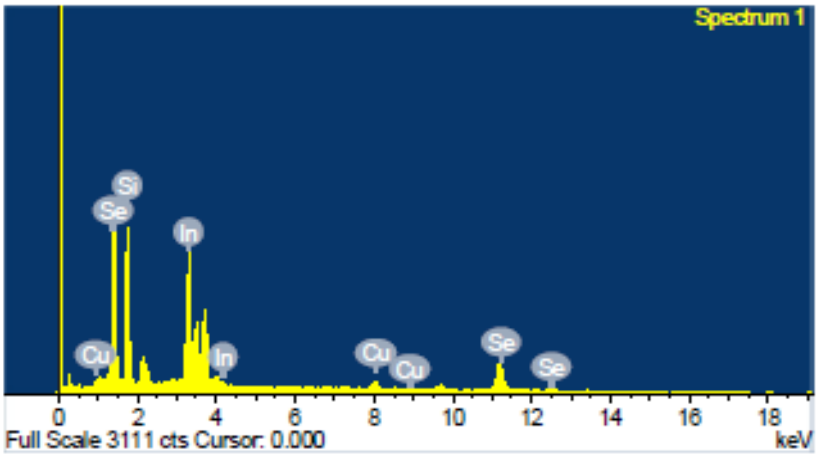

Figure (5): EDX spectrum of $CuInSe_2$ NCs film

Moreover, Fig. (5) shows a typical EDX spectrum of $CuInSe_2$ NCs film which gives atomic concentration Cu/In/Se composition 23.5:24:52.5 closes to the desired 1:1:2 ratio of $CuInSe_2$. Meanwhile, Fig. 6 shows top view SEM image of the as-deposited $CuInSe_2$ thin film (on ITO substrate) using vacum thermal evaporation. As we can see, small lens-shaped spots appear in the SEM image with average size around 100 nm. Interestingly, the observed nanocrystals look homogenous and well distributed on the substrate surface

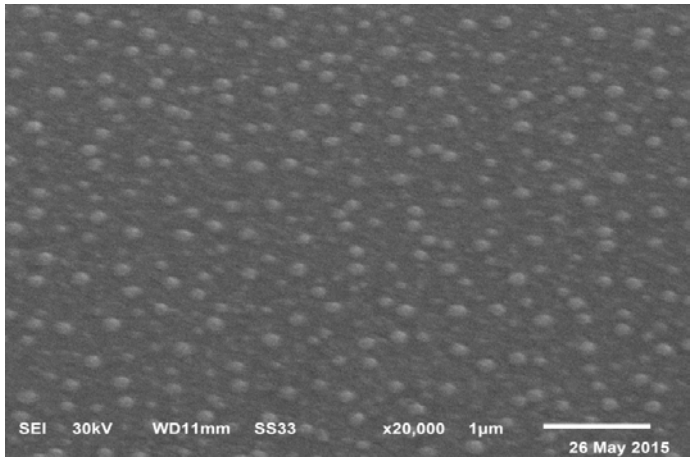

Figure (6): SEM images of our grown CIS NCs thin film which was thermally evaporated on ITO coated glass substrate.

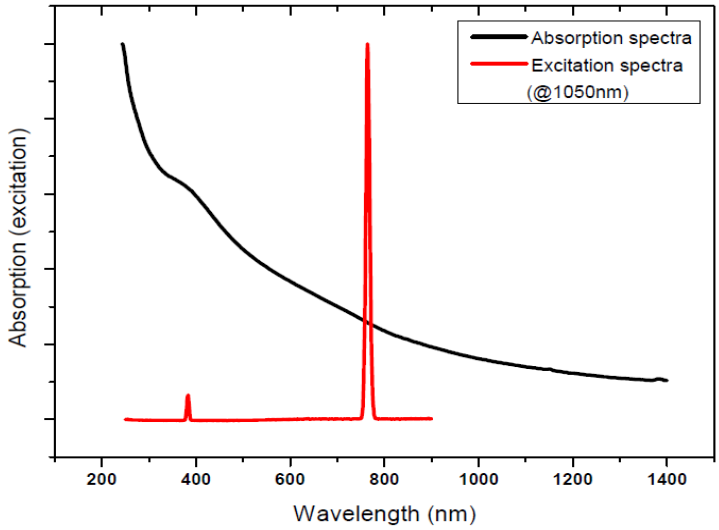

Figure (7): Room temperature optical absorption (black) and excitation spectra (red) of $CuInSe_2$ nanocrystals sample.

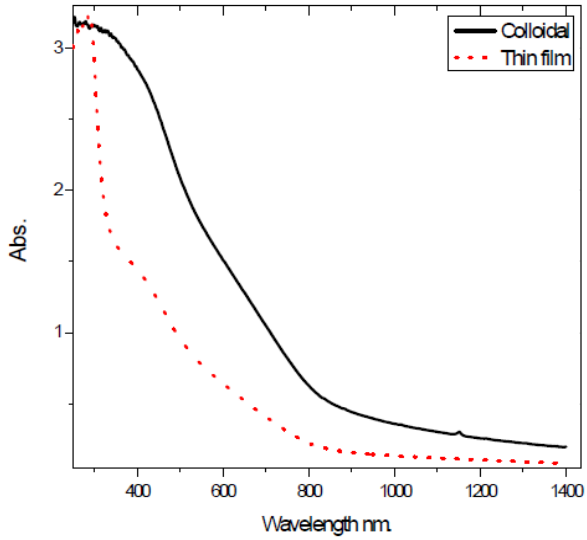

Figure (8): Absorption spectra of $CuInSe_2$ colloidal noanocrystals either in the form of powder (solid line) or evaporated-film (dotted line).

3.3. Optical characterization

The as-synthesized $CuInSe_2$ NCs are well dispersed in hexane and exhibit a dark black colour due to the strong absorption at near infrared wavelengths. The properties of the $CuInSe_2$ NCs have been studied also using optical absorption measurements. Figure 7 shows absorption and excitation spectra of the grown CIS NCs which were dispersed in hexane. As we see the absorption edge of the NCs appears around 1050 nm (corresponds to E_g=1.03eV). This value matches very well to what is reported in literature about the band gap of CIS material [12-15].

The peaks at 750 nm and 380 nm in the excitation spectra confirm their identity to be related to higher energy excited states transitions in the CIS NCs. Fig. (8) shows the absorption spectra of CIS NCs dispersed in hexane and that of CIS film. The two spectra look very similar which reflects the high optical quality of the deposited film along with the well distribution of the CIS NCs when evaporated and condensed on the ITO substrate by thermal evaporation.

3.3.1. Determination of the optical constants of CIS NCs thin film

We have developed software to determine the optical constants of thin films using Transmittance (T) and Reflectance (R) measurements. The model which we used is a modified model of the theory introduced for the first time by Y. Hishikawa *et al.* [11]. In this theory, the optical absorption coefficient α of thin films is determined with high accuracy, from transmittance *(T)* and reflectance *(R)* data using the ratio *T/(1-R)*. The unique thing in this theory-compared to other convential methods based on optical interference effect- is that it can be used to determine the optical constants even for very thin films. It should be mentioned that the optical interference effect is widely used to determine the thickness and other optical constants of relatively *thick* films (>300 nm), but very few groups in the thin film research community who were able to determine the optical constants of very *thin* layers. In the following we summarize our modified theory:

As mentioned in [11], the optical absorption coefficient α of thin films is determined from transmittance *T* and reflectance *R* by using *T/(1-R)*. α can be derived from a numerical fitting between experimental *T/(1-R)*, and theoretical *T/(1-R)*. The expression of *T*, *R*, and *T/(1-R)*, for the structure in Fig.9 are expressed as in the following:

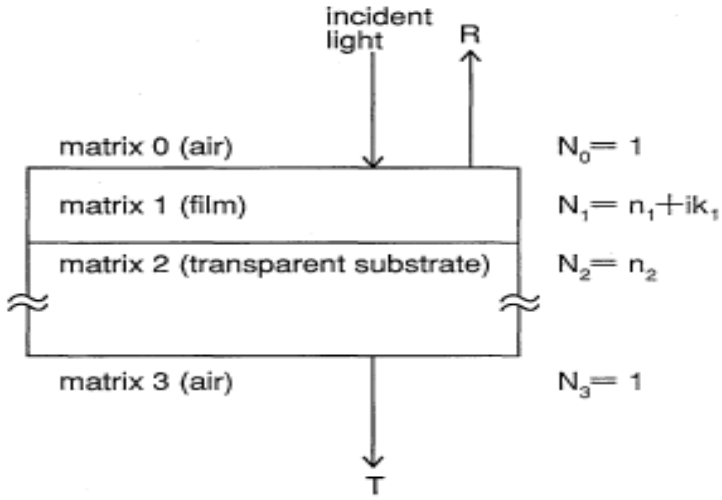

Figure (9): Schematic structure of the incident transmitted and reflected light for measurements of T and R and for the determination of optical absorption coefficient of CIS films [11].

N_k denotes the complex refractive index matrix *k*.

$$T = \frac{T_{23}T_{02}}{1 - R_{20}R_{23}} \tag{1}$$

$$R = \frac{T_{20}^2 R_{23}}{1 - R_{20}R_{23}} + R_{02} \tag{2}$$

$$\left(\frac{T}{1-R}\right)^{-1} = \frac{1 - R_{02}}{T_{23}T_{02}} - \frac{R_{23}}{T_{23}}\left(T_{20} + R_{20}\frac{1 - R_{02}}{T_{02}}\right) \tag{3}$$

Here

$$T_{02} = T_{20} = \frac{n_2}{n_0}\left|\frac{e_1 t_{01} t_{12}}{1 - e_1^2 r_{10} r_{12}}\right|^2, \qquad R_{02} = \left|r_{01} + \frac{e_1^2 t_{01} t_{10} r_{12}}{1 - e_1^2 r_{10} r_{12}}\right|^2$$

$$R_{20} = \left|r_{21} + \frac{e_1^2 t_{21} t_{12} r_{10}}{1 - e_1^2 r_{10} r_{12}}\right|^2, T_{23} = \frac{n_3}{n_2}|t_{23}|^2, \quad R_{23} = |r_{23}|^2$$

$$e_1 = \exp\left(\frac{2i\pi N_1 d}{\lambda}\right) \tag{4}$$

$$t_{kl} = \frac{2N_k}{N_k + N_l}, \qquad r_{kl} = \frac{N_k - N_l}{N_k + N_l}$$

$N_k = n_k + iK_k$: *complex refractive index of matrix k.*

For a typical value of n_2=1.5, We have confirmed that the second term of Eq. (3) is less than 2% of the first term. Therefore Eq. (3) can be rewritten as:

$$\left(\frac{T}{1-R}\right)^{-1} = \frac{1 - R_{02}}{T_{23}T_{02}} = \frac{n_0(1 - |r_{01}|^2)(e^{\alpha d} - e^{-\alpha d}|r_{12}|^2)}{n_3|t_{01}|^2|t_{12}|^2|t_{23}|^2} + \frac{4n_0|r_{01}||r_{12}|\sin(\theta + \gamma_{12})\sin(\gamma_{10})}{n_3|t_{01}|^2|t_{12}|^2|t_{23}|^2} \tag{5}$$

Here, $\theta = \frac{2\pi n_1 d}{\lambda}$, λ: *wavelength*, *d: film thickness*

$\gamma_{12} = \arg(r_{12})$, $\gamma_{10} = \arg(r_{10})$,

The second term of Eq. (5) which includes interference as $\sin(\theta + \gamma_{12})$ is much smaller than the first term when $k_1 << 1$, because $\sin(\gamma_{10}) \cong \frac{2k_1}{n^2 - 1}$. Thus it has been confirmed that the interference effect in T/(1-R), is very small when $k_1 << 1$. In contrary to what Y. Hishikawa *et al*. did in their work, we put n_1 (real part of refractive index of the film) with rough value for the whole wavelength range (between 0.5-2) without limitation to the corresponding values of maxima or minima in the spectra. This way and when the experimental value of *T/(1-R)* are known,can be determined from Eq. (3) by any iteration calculation. When we put rough values of (n_1) and (*d)* in the calculation, α is iteratively determined using Eq. (3) from *T/(1-R)*, n_1 and *d*. Next, the values of n_1 at all wavelengths are also iteratively determined by Eq. (1) or Eq. (2) from *(T)* or *(R)* and *(d)*. At these wavelengths, Eq. (4) should be used in calculation to determine n_1 iteratively by comparing experimental *(T)* with theoretical *(T)*. Finally, Eq. (2) is used to

calculate reflectance (R') from determined α and n_1. R' and experimental R are then compared in order to check whether, n_1 and d are properly determined. If R' and R do not agree well, we adjust the value of d, and the same procedure is carried out until good agreement is obtained. We found that the theoretical error in T and R is less than $\pm 0.1\%$ at all wavelengths used in calculation. The optical absorption coefficient (α) of the coated CIS thin films has been estimated from both the transmittance (T) and Reflectance (R) measurements using UV-VIS-IR technique. The results are shown in Figs.(10,11). As we can see, the calculated T and R according to the model which we have developed, match perfectly with the experimental data of (T) and (R) (see Fig.10). This confirms the validity of our model. From our model, we were able to extract the values of (α) (Fig.11) and the band gap of the CIS film (inset of Fig.11). A band gap (E_g) of nearly 1 eV is extracted from Fig.11, where $(\alpha h\nu)^2$ is plotted against energy. This value of E_g is quite acceptable value for CIS materials. Remarkably, we have obtained (α) of the CIS film as high as ~$3x10^5$ cm^{-1}. To the best of our knowledge, this value of (α) can be considered as one of the highest value of the optical absorption coefficient obtained so far in literature for CIS thin film grown by colloidal chemistry. This may open the door towards improvement of the overall quantum efficiency of CIS-based colloidal solar cells.

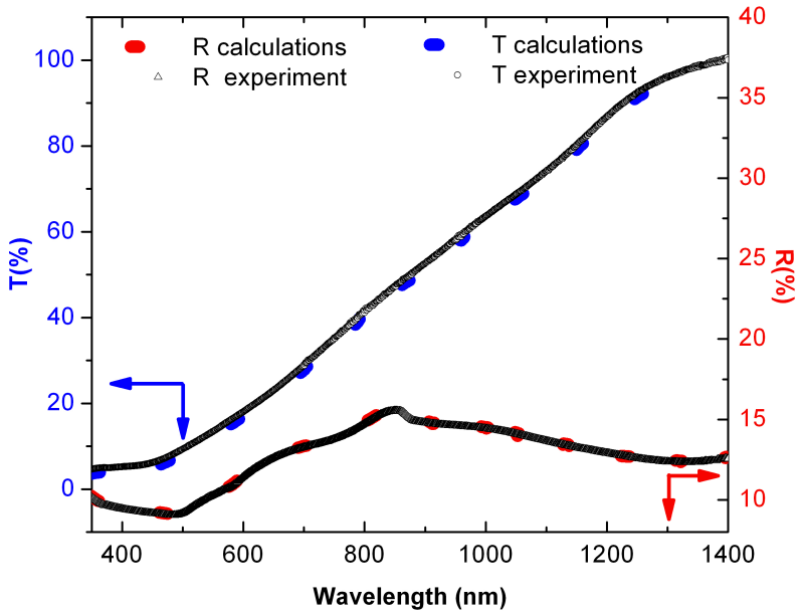

Figure (10): Experimental (points) and calculated (lines) Transmittance (T) and Reflectance (R) spectra of CIS nanocrystaline films.

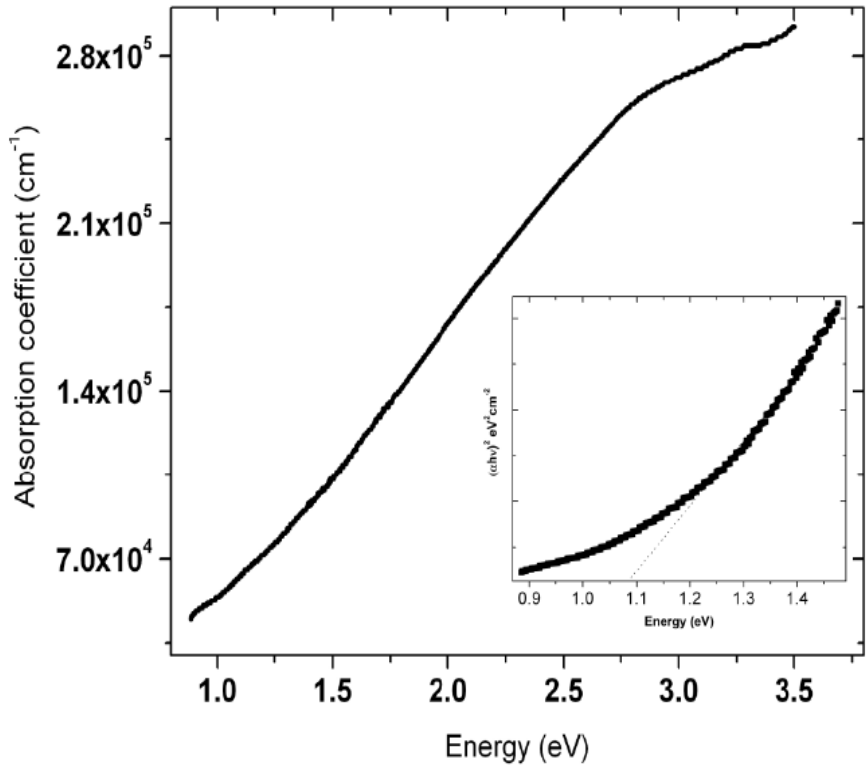

Figure (11): Calculated optical absorption coefficient of CuInSe nanocrystaline film from transmittance and reflectance data based on our developed modeling. The inset shows variation of $(\alpha h\nu)^2$ against energy for CuInSe film. From extrapolating the linear part of the curve we can determine a band gap value of ~1.09 eV.

3.4. Effect of Thermal Annealing on CIS NCs Film

3.4.1. Influence of annealing on the structural properties of the CIS film

In order to study the influence of thermal annealing on the structural and optical properties of the deposited CIS NCs film, we measured both XRD and EDX patterns of different annealed samples at various annealing temperatures with fixed annealing time of 5 min. Fig. (12) shows XRD of CIS powder compared to that when deposited in thin film form at different annealing temperatures up to 300^0C. As we can as annealing temperatures increases a small peak around 44^0 appears. This small peak corresponds to XRD of "Cu" metal which indicates that as annealing temperature increases a deviation from the sticiometric conditions is more likely[16-19]. This hypothesis was confirmed by corresponding EDX measurements as can be seen in table 1. Interestingly we find that the Cu/In ration increases with annealing. This might be due to the fact that some quantity of In would be lost during annealing at T > 250 ^{0}C as melting point of In is only 150°C [20]. Fig. (14) shows SEM micrographs of the prepared CIS films, annealed at different temperatures.

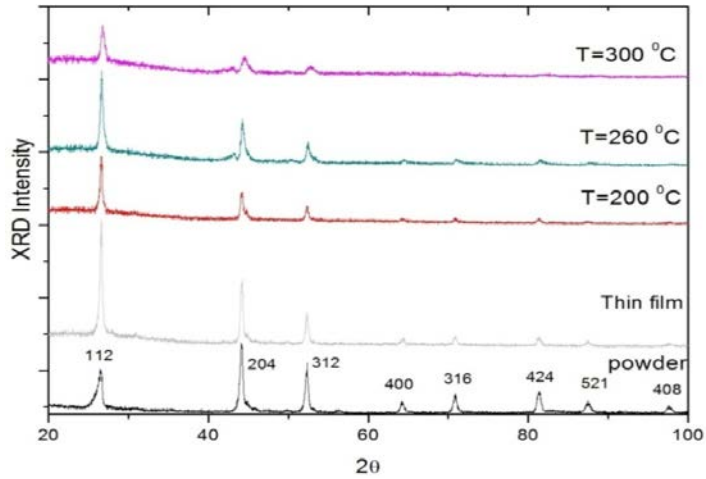

Figure (12): XRD pattern of $CuInSe_2$ sample in powder and thin film form at room temperature (lower two spectra). The above three spectra refers to annealed thin film of the same sample at different annealing temperatures (200, 260 and 300^{0}C).

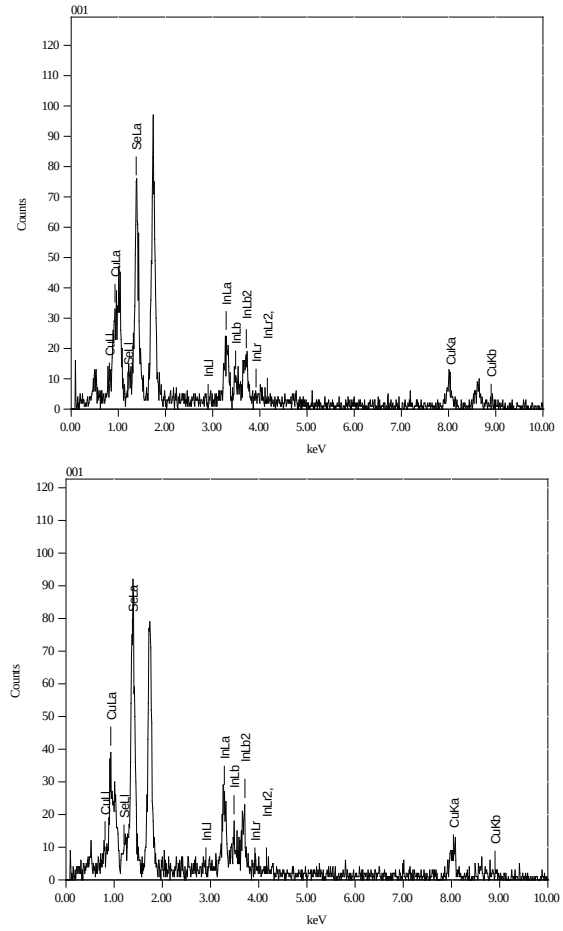

Figure (13): EDX spectra of different CIS samples annealed at: 326 ^{0}C (left), and 346^{0}C (right)

Table (1): Atomic concentration in percentage

Sample name	T(^{0}C)	Cu	In	Se	Cu/In
CIS22	326	21.18	23.08	55.74	0.91
CIS23	341	20.59	21.87	57.55	0.94
CIS25	346	25.97	21.96	52.06	1.18

First we note from the SEM images that for the annealed films, the surface is uniform, homogeneous, continuous and without voids. We can see also from Fig.14 that the grains are merged in each other and their size grades increase with the increase in the annealing temperature. Some white color particles are seen on the surface of annealed films at 345 ^{0}C which may be related the presence of excess "Cu" [21-23].

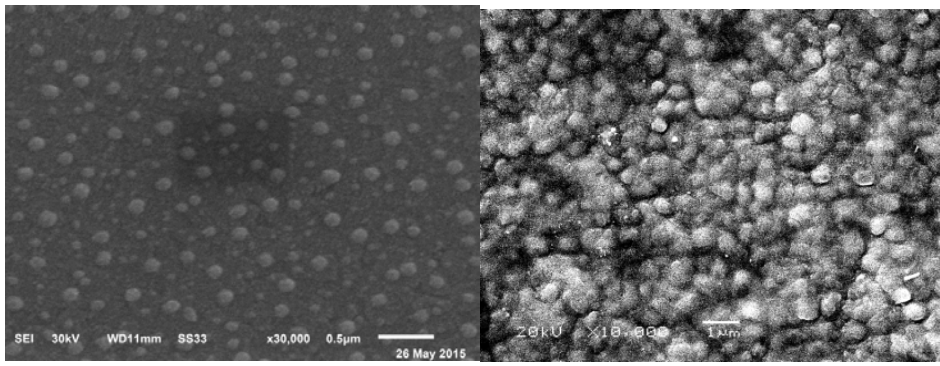

(a) (b)

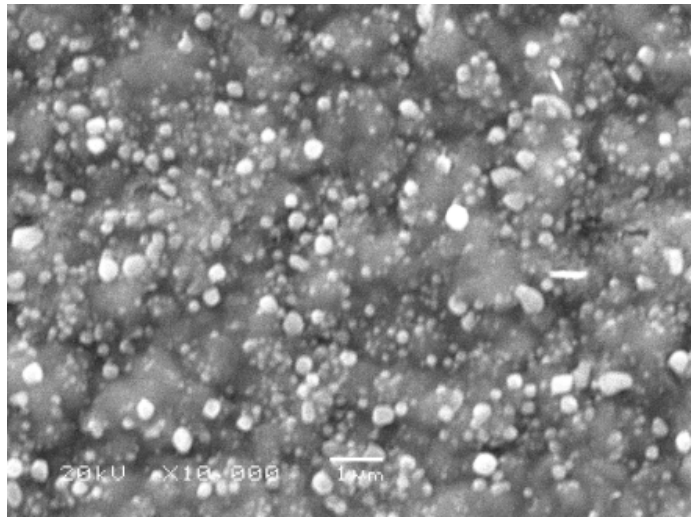

(c)

Figure (14): SEM micrographs of CIS annealed at different temperatures: (a) as-deposited (b) 326^{0}C and (c) 345^{0}C.

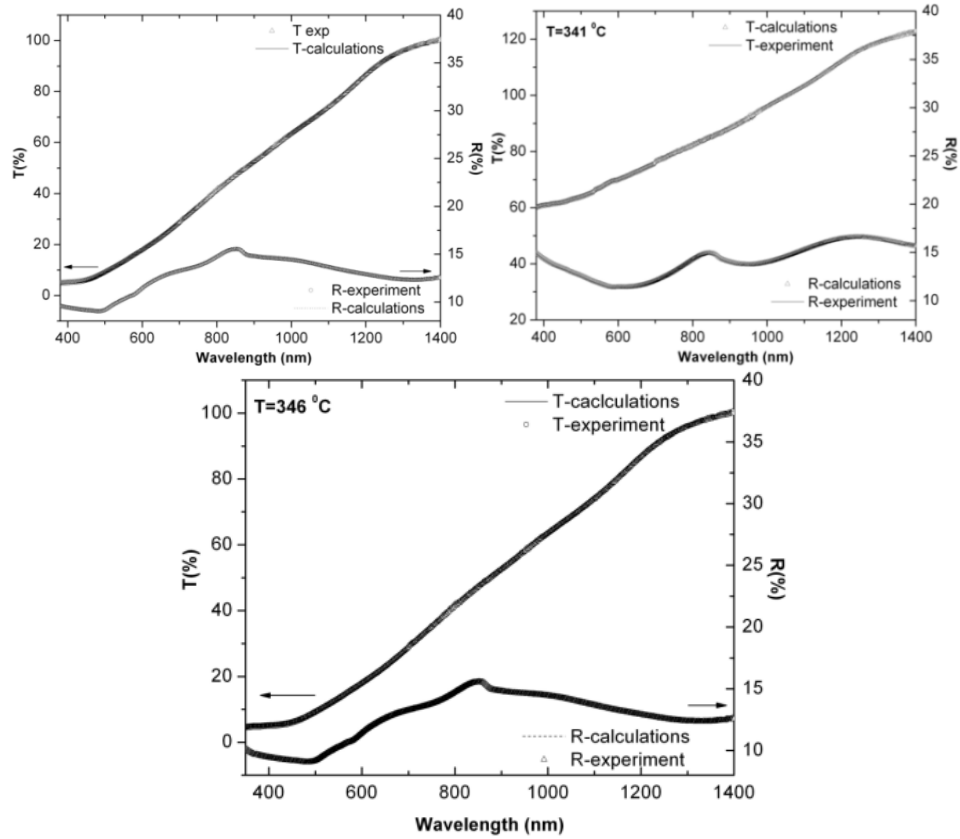

Figure (15): Experimental (points) and calculated (lines) transmittance and reflectance spectra of CIS films annealed at 326^0C (top), 341^0C (middle) and 346^0C (bottom).

3.4.2. Influence of annealing on the Optical properties of CIS thin films

Figure (15) shows the experimental and calculated T and R of different CIS film where the effect of annealing on the optical properties is studied. According to our model we estimated the absorption coefficient, α, of the annealed films of photon energy. The films have values for α of the order 10^5 cm^{-1}, indicating that the material is of the direct-band-gap type and that transition is allowed [4]. It is seen that the films have higher absorption coefficient ($\alpha \approx 5x\ 10^{-5}$ cm^{-1}) when it annealed at 346◦ C. The annealing increases the absorption coefficients, this influence was due to an improvement in compositional uniformity [4]. It was found that the absorption coefficient varied in a systematic manner with the Cu/In ratio over all the wavelength range. The similar results have been reported by S.M. Firoz Hasan et al. and K.G. Deepa et al. for $CuInSe_2$ thin films [23,24]. The energy gap is one of the most important parameters in producing solar cells. The absorption coefficient, α, is related to the energy gap, E_g, according to the equation:

$$\alpha\, h\nu = A(h\nu - E_g)^n$$

where E_g is the optical energy gap, A is a constant and n= 1/2 or 2 for an allowed direct, or indirect-transition energy gap, respectively. As in Fig. 16 the energy gaps were calculated by noting the y-axes intercept when $(\alpha h\nu)^2$ is plotted against ($h\nu$). The energy band gap of annealed red shifted (1.09 –1.8 eV) due to annealing. Furthermore, the linear nature of the plots through the absorption range indicates that $CuInSe_2$ compound has a direct band gap after annealing [1]. A variation in the Eg was noted with variation in Cu/In ratio for the samples where 1.1 and 1.03 eV for Cu/In ratios of 0.91, and 1.18, respectively. It is seen that more indium-rich films have higher energy gaps than less indium-rich ones. If the In/Cu ratio increases, indium occupies some of the copper sites, resulting in anti-site defects. The size of the indium atom is larger than that of copper. Hence, this type of defect would increase the band gap [11]. The energy gaps show that the less copper-rich samples have higher energy gaps

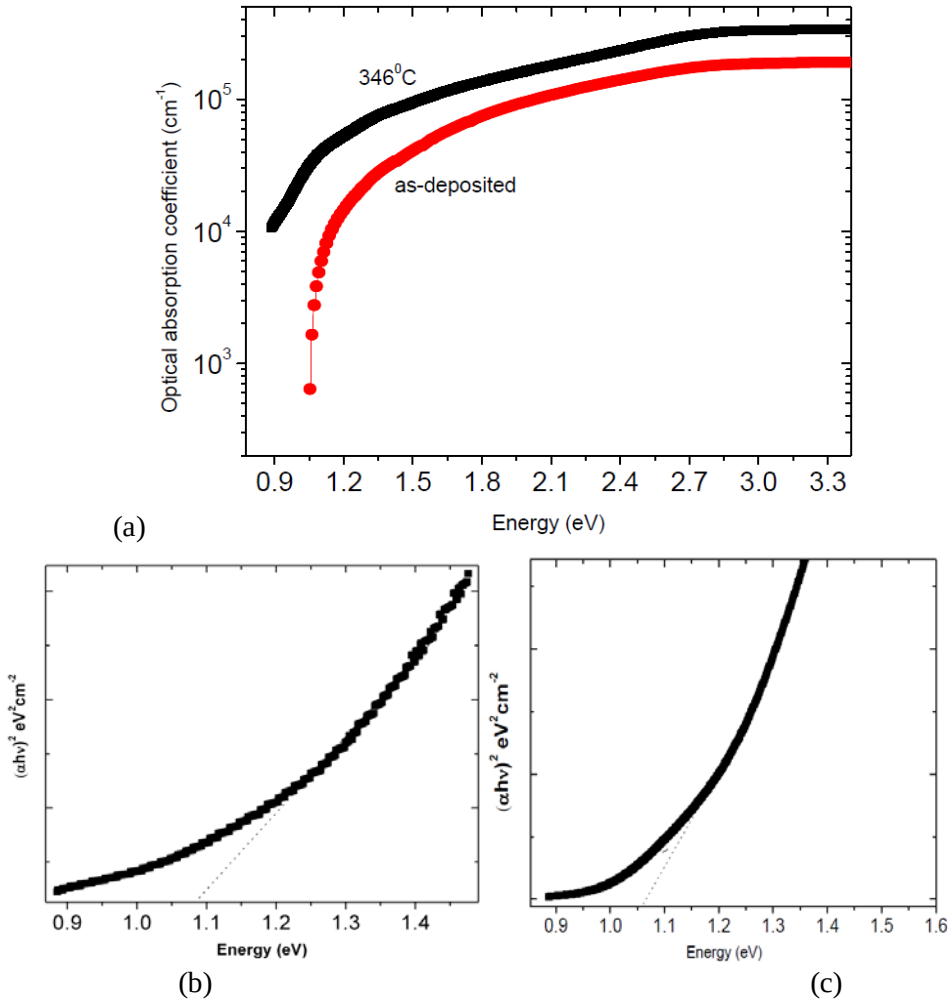

Figure (16): (a) Variation of the absorption coefficient of CIS films with annealing. (b) Determination of E_g of as-deposited CIS film. (c) Eg of CIS film annealed at 346^{0}C.

than the more copper-rich ones. In the case of I–III–VI2 compounds, the uppermost valence bands get strongly influenced by the metal d levels (in the present case Cu-d levels). The Cu-3d levels and Se-4p levels being degenerate and possessing same symmetry because of the p–d hybridization interaction, the valance band maxima can be displaced upwards. Hence an increase in Cu content could increase the spread of Cu-3d orbitals, which enhanced the possibility of interaction leading to the reduction of the E_g [16]. The similar results have been reported by S.M. Firoz Hasan et al. [20] and K.G. Deepa et al. [21] for $CuInSe_2$ thin films. The band gaps energy obtained in this work fall in the range that is optimal for conversion of solar radiation (Eg= 1.04–1.7 eV) [22-23].

5. Conclusions

In summary, nanocrystals of tetragonal phase of $CuInSe_2$ have been synthesizes via a simple, low- cost wet chemistry method. As-synthesized $CuInSe_2$ NCs in the shape of nanoparticles well crystallized with a nearly uniform morphology. The EDX measurements confirm that obtained films are $CuInSe_2$ stoichiometrically. Also XRD and TEM measurements confirm that the as-grown NCs are polycrystalline tetragonal $CuInSe_2$. Moreover, a CIS NCs thin film from these nanocrystals was deposited by vacum thermal evaporation technique. The films show high optical quality when thermally annealed in vacum at temperatures up to 346^0C, for relatively short period of annealing time (5 minutes). A remarkable enhancement of the absorption coefficient ($\sim 3X10^5$ cm^{-1}) of the formed CIS films was found when the annealing temperatures increases until it reaches $T=346^0$C. Compared with vacum-based techniques, solution-based methods offer low-cost and scalability advantages of producing CIS material. Fabrication of thin film solar cells using solution-based processes are expected to be a potential substitute for vacum-based technology of thin film solar cells.

Acknowledgments

The author is grateful to Prof. Mostafa El-Nimr, Tanta University, for excellent technical help during building the laboratory of Nanophotonics, and for fruitful discussions. Financial support from Science and Technological Development fund (STDF) through project with contract No. 4333 (Young Research Grant) is highly appreciated.

References

1. Ingrid Repins, Miguel A., *Prog. Photovolt: Res. Appl*. **16**, 235 (2008).
2. R. Marquez, C. Rincon, *Sol. Energ. Mat. Sol*., C., **71**, 19 (2002).
3. T. V. Kuznetsova, V. I. Grebennikov, H. Zhao, C. Derks, C. Taubitz, *Appl. Phys. Lett*. **101**, 111607 (2012).
4. H. P. Wang, I. Shih, C.H. Champness, *Thin Solid Films*, **361**, 494 (2000).

5. G. Arangurena, E. Hernandeza,, A. Lopez Pescadorb, C.A. Durante Rincona, Maximo Leon, *Materials Letters*, **58**, 573 (2004).

6. M. León, 1, R. Serna, S. Levcenko, A. Nateprov, A. Nicorici, J. M. Merino, and E. Arushanov, *Phys. Stat. Sol*. (a) **203**, 11, 2913 (2006).

7. Se Hankwon, S. Park, B. Ahn, K., *Yoon and J. Song, Solar Energy*, **64**, 1, 55 (1998).

8. G. Ariswan, M. Elhaj Moussa, F. Abdelali, C. Guastavino, L. linares, *Solid State Commun*, **124**, 391 (2002).

9. Antoine de Kergommeaux, Angela Fiore, Jer´ome Faure-Vincent, Adam Pron and Peter Reiss. Adv. Nat. *Sci.: Nanosci. Nanotechnol*., **4**, 015004 (2013).

10. B. D. Cullity and S. R. Stock, Elements of X-ray Diffraction (Prentice-Hall, Saddle River), NJ, **3**rd ed., p. 264 (2001).

11. Y. Hishikawa, N. Nakamura, S. Tsuda, S. Nakano, Y. Kishi, and Y. Kuwano, *Jpn. J. Appl. Phys*., **30**, 1008 (1991).

12. J.M. Merino, M. Di Michiel, M. Leo´n, *Journal of Physics and Chemistry of Solids*, **64**, 1649 (2003).

13. H. Z. Xiao, L.Chung Yang, and A. Rockett, *J. Appl. Phys*., **76**, 1503 (1994).

14. H. P. Wang, I. Shih, and C. H. Champness, *Thin Solid Films*, **494**, 361 (2000).

15. C. Rincón, S. M. Wasim, G. Marn, and I. Molina, *J. App. Phys*., **93**, 780 (2003).

16. Jian Liu, Shuyan Shao, Gang Fang, Bin Meng, Zhiyuan Xie, Lixiang Wang, *Adv. Mate*., **24**, 2774 (2012).

17. S. H. Wei, S. B. Zhang, and A. Zunger, *J. Appl. Phys*., **85**, 7214 (1999).

18. Mahesh Chand Sharma, Balram Tripathi, Sumit Kumar, Subodh Srivastava, Y.K. Vijay. *Materials Chemistry and Physics*, **131**, 600 (2012).

19. A. Ashour, A.A.S. Akl, A.A. Ramadan, N.A. El-Kadry, K. Abd El-Hady., *Materials Science and Engineering*, B **134**, 63 (2006).

20. S.M. Firoz Hasan, M.A. Subhan, Kh.M. Mannan., *Optical Materials*, **14**, 329 (2000).

21. K.G. Deepa, P.M. Ratheesh Kumar, C. Sudha Kartha, K.P. Vijayakumar. *Solar Energy Materials & Solar Cells*, **90**, 3481 (2006).

22. S.N. Kundu, D. Bhattacharyya, S. Chaudhuri, A.K. Pal., *Materials Chemistry and Physics*, **57**, 207 (1999).

23. Angela Fiore, Nicolas Bruyant, Fre´de´ric Chandezon, Peter Reiss, Adam Pron, Re´mi de Bettignies, Je´rˆome Faure-Vincent, *Solar Energy Materials & Solar Cells*, **95**, S39 (2011).